Research Article | Vol. 32, No. 19 / 9 Sep 2024 / Optics Express 33950

Optics EXPRESS

Nonlinear Thomson scattering: velocity asymmetry inherent in electron figure-8 motion

MAHONRI ROMERO,[1] LUKE ROBINS,[1] ARIA STEVENS,[1] NUNO SA,[2] YANCE SUN,[1] MICHAEL WARE,[1,3] AND JUSTIN PEATROSS[1,4]

[1]Dept. of Physics and Astronomy, Brigham Young University, Provo, Utah 84602, USA
[2]University of the Azores, Portugal
[3]ware@byu.edu
[4]peat@byu.edu

Abstract: The individual polarization components of nonlinear Thomson scattering arise from the separate dimensions of electron figure-8 motion caused by a linearly polarized laser field. We present the first measurements of nonlinear Thomson scattering in both emission hemispheres. In the electron average rest frame, the shape of the electron figure-8 path is symmetric about the laser polarization dimension. However, the periodic electron velocity is intrinsically asymmetric. The full scattering emission pattern reveals this asymmetry and the direction that electrons move around the figure-8 path.

1. Introduction

Much theoretical effort has been devoted to understanding nonlinear Thomson scattering [1–19], while comparatively few experimental observations have been made of the phenomenon. Most measurements employ energetic electron beams that collide with intense laser pulses [20–27], which maps the Thomson scattering into a highly-directional beam of blueshifted x-rays. Only a handful of experimental measurements have been made in a frame of reference that does not differ strongly from the electron average rest frame [28–32]. Experiments are hampered by the low cross section of electron-photon interactions and the associated challenge of reaching sufficient density of free electrons without confounding effects of interactions between electrons and ions present. Prior to our recent work [33,34], only one experimental study, Chen et al. [29], measured the spatial structure of nonlinear Thomson emission. They observed second and third harmonic light scattering patterns in the plane perpendicular to laser propagation and compared the measured data with a theoretical prediction for a single polarization component of the scattered light.

Landau and Liftshitz pointed out in 1951 that electrons should execute figure-8 motion in a linearly polarized plane wave when there is sufficient amplitude to drive relativistic motion [1], as illustrated in Fig. 1. In 1962, Vachaspati showed that electrons experiencing such motion should scatter both odd and even harmonics, referred to as *nonlinear* Thomson scattering [2]. In 1968, Eberly and Sleeper showed that the rising edge of the laser pulse causes electrons that are initially at rest to acquire a forward drift as they oscillate in the laser field, responding to both the electric and magnetic parts of the Lorentz force [3]. In 1970, Sarachik and Shappert published a comprehensive theoretical treatment of nonlinear Thomson scattering in a frame that drifts along with the electron [4].

We recently published the first polarization-resolved measurements of nonlinear Thomson scattering, for fundamental, second-harmonic, and third-harmonic scattered photons [33,34]. We used single-photon counting to measure light scattered from free electrons in an intense laser focus (800 nm wavelength with peak intensity 2×10^{18} W/cm^2). However, like the Chen measurements, those observations were restricted to a plane perpendicular to laser propagation.

#524524 https://doi.org/10.1364/OE.524524
Journal © 2024 Received 21 Mar 2024; revised 24 Aug 2024; accepted 26 Aug 2024; published 5 Sep 2024

Optics EXPRESS

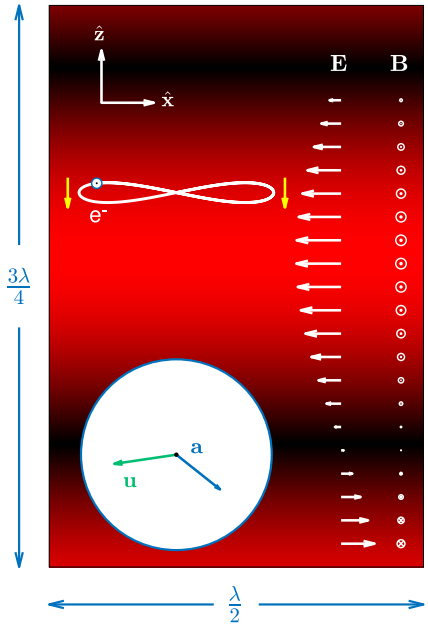

Fig. 1. Animation of an electron trajectory in a linearly polarized plane wave with $\alpha = 1$ in the electron average-center-of-mass frame (see Visualization 1). The electron trajectory is to scale with the wavelength of the plotted laser field (shown with arrows and shading). The inset shows the velocity and the acceleration of the electron, where the radius of the circle corresponds to the speed of light c for velocity and $1.25\omega c$ for acceleration, where ω is the angular frequency of the driving field.

In our previous analysis, we demonstrated that the x-dimension of the figure-8 electron motion (parallel to linear polarization, see Fig. 1) gives rise to scattered photons with one polarization, while the z-dimension gives rise to scattered photons with an orthogonal polarization, as measured in a plane perpendicular to the laser propagation. By measuring both polarizations, we confirmed the two-dimensional nature of the figure-8 motion. Previous observations, while consistent with the electron figure-8 motion, were also consistent with *hypothetical* electron motion constrained to oscillate in only a single dimension.

Here we report on scattered fundamental, second, and third harmonic light measured over nearly the full emission sphere. At each angle in the emission sphere, we resolve the scattered light into orthogonal polarization components corresponding to azimuthal and longitudinal lines. By measuring the entire sphere, as opposed to the previous measurements made only the directions perpendicular to the laser, we are able to more fully characterize the motion of the electrons scattering the light and definitively confirm the predicted figure-8 motion.

Figure 2 shows calculated far-field emission patterns fundamental, 2nd harmonic, and 3rd harmonic over the entire emission sphere. The calculations are based on the theoretical analysis of Sarachick and Shappert [4], as outlined in our previous publication (see Eq. (8) in [33]). The scattered light is computed in the average rest frame of an individual electron that experiences a plane wave traveling in the $+z$ direction (the laser propagation direction, shown as 'north' in Fig. 2) and polarized along the x direction. In our experiment, we measure light around 'latitude' lines defined by $\theta = 30°$, $45°$, $60°$, $75°$, $90°$, $105°$, $120°$, and $135°$, where 'north' corresponds to $\theta = 0°$ and the equatorial plane corresponds to $\theta = 90°$. The left column of Fig. 2 shows emission of light that is polarized along 'latitude' lines and the right column shows light polarized in the 'longitude' lines of the emission sphere.

Optics EXPRESS

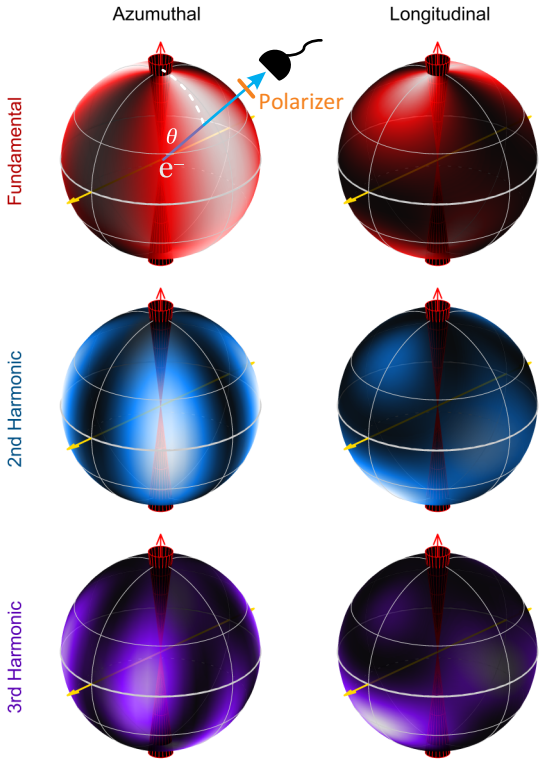

Fig. 2. Animation showing the far-field emission pattern for fundamental (top), 2nd harmonic (middle), and 3rd harmonic (bottom) scattered light (see Visualization 2). The left column shows the azimuthal polarization component of the scattered light, while the right column shows the longitudinal component. The intensity of the driving plane-wave field is set to 2×10^{18} W/cm^2. The laser propagation direction is indicated by the arrow at the 'north' pole, while laser polarization direction is indicated by arrows coming out the 'equator'.

The visualization associated with Fig. 2 shows an animation of the emission spheres rotated to show emission in all directions and in both hemispheres. Examination of the animation shows a strong asymmetry between the emission patterns of the 'northern' and 'southern' hemispheres of the emission sphere. Specifically, note that there is significantly more emission in the southern hemisphere than the northern hemisphere for longitudinally-polarized 2nd and 3rd harmonic emission. This asymmetry arises because electrons move in the same direction at both ends of the figure-8 trajectory, opposite laser propagation as indicated by the yellow arrows in Fig. 1. The acceleration of the electron is greater on the outside edges of the figure-8, so that emission is stronger during this portion of the trajectory. Radiation is directed more in the direction of this motion so that this asymmetry causes electrons to emit much more longitudinally polarized light into the southern hemisphere. We report here the first measurements of this asymmetry. This not only confirms the unique midpoint-crossing geometry of the figure-8 motion, but it also demonstrates the direction of travel that the electron takes around the figure-8 trajectory.

2. Formalism

We summarize here the classical electromagnetic theory that we use to model nonlinear Thomson scattering from individual free electrons in a tight laser focus. We start with the classical equation

Optics EXPRESS

of motion for a point charge. Under the influence of electric and magnetic fields, $\mathbf{E}$ and $\mathbf{B}$, an electron responds to the Lorentz force

$$\frac{d\mathbf{p}}{dt} = q\left(\mathbf{E} + \frac{\mathbf{p}}{m\gamma} \times \mathbf{B}\right), \tag{1}$$

where m, q, and $\mathbf{p}$ denote the electron mass, charge, and momentum, respectively, and the Lorentz factor is $\gamma = \sqrt{1 + p^2/(mc)^2}$. Radiation reaction is neglected. The dimensionless parameter $\alpha = qE/\omega mc$ specifies the field strength.

The vector field of an idealized laser focus is given by

$$\mathbf{E} = \mathrm{Re}\left\{E_0 e^{-\left(\frac{\tilde{\varphi}}{\omega\tau}\right)^2}\left(\hat{\mathbf{x}} + \frac{xy}{2\mathbb{Z}^2}\hat{\mathbf{y}} - i\frac{x}{\mathbb{Z}}\hat{\mathbf{z}}\right)\frac{z_0}{\mathbb{Z}} e^{-\frac{kz_0\rho^2}{2|\mathbb{Z}|^2}} e^{i\tilde{\varphi}}\right\}, \tag{2}$$

where z_0 is the Rayleigh range, ρ the axial radius, τ the pulse duration, $\mathbb{Z} = z_0 + iz$, and $\tilde{\varphi} = kz[1 + \rho^2/(2|\mathbb{Z}|^2)] - \omega t$ [35,36]. The associated magnetic field is $c\mathbf{B} = \hat{\mathbf{x}}E_y + \hat{\mathbf{y}}E_x + \hat{\mathbf{z}}yE_z/x$. In the limit $z_0 \to \infty$ and $\tau \to \infty$, this expression reduces to a plane wave like that used to generate Figs. 1 and 2.

A randomly placed electron is assumed to break free from an atom or ion when the local intensity of the rising edge of the laser pulse exceeds the ionization threshold, with initial momentum $\mathbf{p}_0 = 0$. The electron's subsequent trajectory is then calculated using Eqs. (1) and 2. Once position $\mathbf{r}(t)$ and momentum $\mathbf{p}(t)$ are numerically obtained for the trajectory, ordinary electron velocity and acceleration are obtained from $\mathbf{u}(t) = \mathbf{p}/(m\gamma)$ and $\mathbf{a}(t) = \frac{q}{\gamma m}\left[\mathbf{E} + \mathbf{u} \times \mathbf{B} - \mathbf{u}(\mathbf{u} \cdot \mathbf{E})/c^2\right]$ [37].

With the electron trajectory in hand, the far-field scattered radiation is computed using [37]

$$\mathbf{E}_{\mathrm{rad}} = \frac{q}{4\pi\epsilon_0 c^2 R} \frac{\hat{\mathbf{R}} \times \left((\hat{\mathbf{R}} - \mathbf{u}/c) \times \mathbf{a}\right)}{\left(1 - \hat{\mathbf{R}} \cdot \mathbf{u}/c\right)^3}, \tag{3}$$

where R is the distance to the detector, and $\hat{\mathbf{R}} = \hat{\mathbf{x}}\sin\theta\cos\phi + \hat{\mathbf{y}}\sin\theta\sin\phi + \hat{\mathbf{z}}\cos\theta$ is a unit vector specifying the direction to the detector, expressed in terms of the usual spherical coordinates. The right-hand side of (3) is evaluated at (retarded) time t, whereas the left-hand is a function of detector time $t' = t + \frac{R}{c} - \hat{\mathbf{R}} \cdot \frac{\mathbf{r}}{c}$.

We resolve the far-field radiation into orthogonal polarization components, either along unit vector $\hat{\boldsymbol{\theta}} = \hat{\mathbf{x}}\cos\theta\cos\phi + \hat{\mathbf{y}}\cos\theta\sin\phi - \hat{\mathbf{z}}\sin\theta$ or $\hat{\boldsymbol{\phi}} = -\hat{\mathbf{x}}\sin\phi + \hat{\mathbf{y}}\cos\phi$. The total energy per steradian (angular fluence) is $\Phi_\theta + \Phi_\phi$ where $\Phi_\theta = \epsilon_0 cR^2 \int_{-\infty}^{\infty} |\hat{\boldsymbol{\theta}} \cdot \mathbf{E}_{\mathrm{rad}}|^2 dt'$ and $\Phi_\phi = \epsilon_0 cR^2 \int_{-\infty}^{\infty} |\hat{\boldsymbol{\phi}} \cdot \mathbf{E}_{\mathrm{rad}}|^2 dt'$. Experimentally, we employ a polarizer aligned with either $\hat{\boldsymbol{\theta}}$ or $\hat{\boldsymbol{\phi}}$ to measure Φ_ϕ and Φ_θ. The laser propagates along $\hat{\mathbf{z}}$ in accordance with (2). Finally, we apply a spectral window to the Fourier transform of $\mathbf{E}_{\mathrm{rad}}$ to restrict to a specific harmonic. This process is repeated for representative electrons distributed throughout the collection volume and the total radiated signal is found by summing the contributions from each spatial location. Dividing total signal by the corresponding photon energy gives the expected photon counts per steradian at our detector.

3. Experimental setup

Figure 3 gives an overview of the experimental setup. An off-axis parabola focuses 800 nm Ti:sapphire laser pulses to a radius of $w_0 = 3.2\,\mu\mathrm{m}$, corresponding theoretically to $z_0 = 40\,\mu\mathrm{m}$. The pulse duration is measured to be $\tau = 40$ fs (FWHM = 38 fs) and pulse energy 50 mJ. The peak intensity at the center of the focus is estimated to reach 2×10^{18} W/cm^2. Note that 2.1×10^{18} W/cm^2 corresponds to $\alpha = 1$.

Optics EXPRESS

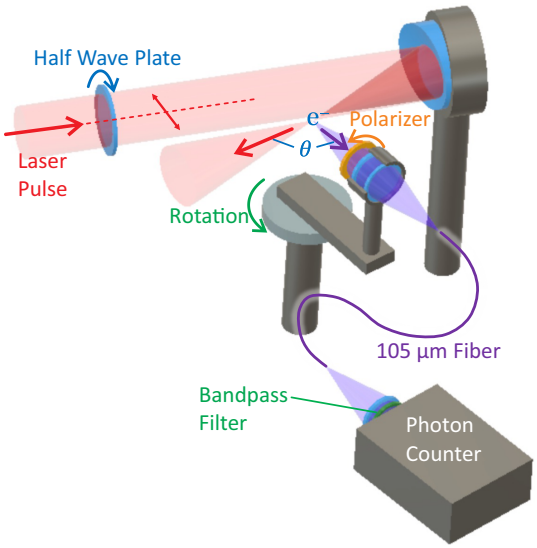

Fig. 3. Experimental setup inside vacuum. An off-axis parabola focuses the laser pulses. A half wave plate rotates the linear polarization of the beam before focusing. Scattered photons traverse a wire-grid polarizer and are imaged into an optical fiber. The photon collection assembly rotates longitudinally.

The goal of this experiment is to measure nonlinear Thomson scattering over much of the emission sphere. Azimuthal rotation of the scattered light is accomplished via rotation of the laser polarization using a half wave plate, with the laser polarization remaining close to linear after reflection from the off-axis parabola. Longitudinal rotation is accomplished by rotating the collection lens setup about a vertical axis that intersects the laser focus. We optimize alignment for maximum signal at each different value of θ.

A 1:1 collection lens (accepting 0.15 steradians) images the interaction region onto the end of a 105 μm fiber optic that leads to the detector. A wire-grid polarizer is placed in front of the collection lens to select the polarization component of the detected light. A 40-nm-wide bandpass filter centered at 900 nm is installed before the detector to measure the (redshifted) fundamental, a 25-nm bandpass filter centered at 450 nm to measure the 2nd harmonic, and a 10-nm bandpass filter centered at 310 nm to measure the 3rd harmonic. The fiber coupling efficiency C, filter transmission T, and detector quantum efficiency η combine for an overall detection efficiency of $CT\eta = 6\%$, 1%, and 0.6% for 1st, 2nd, and 3rd harmonics, respectively.

We use photon counting to measure the scattered light. The laser fires at 10 Hz and individual photons are collected from $N_s = 600$ laser shots at each angle. Our detectors cannot distinguish single photon detection events from multiphoton detections. To correct for this, we assume a Poisson distribution for photons per shot and then correct for multi-photon events using

$$N_{ph} = -N_s \ln\left(1 - \frac{N_{det}}{N_s}\right),$$

where N_{ph} is the corrected number of detected photons given N_{det} detector clicks. The fundamental and second harmonic photons are detected using an avalanche photodiode and the third harmonic using a photomultiplier tube.

Electrons are donated from helium backfilled in the interaction chamber at 5×10^{-4} Torr, 2×10^{-2} Torr, and 1.5 Torr for the 1st, 2nd, and 3rd harmonic, respectively. Helium's two electrons become ionized early during the pulse throughout a large focal region. Compared to the

Optics EXPRESS

ionization region, a relatively small volume in the focus reaches sufficient intensity for nonlinear Thomson scattering, which occurs near the temporal peak of the pulse.

The Lorentz force causes electrons to acquire a forward drift during the rising edge of the laser pulse [3]. This forward drift causes scattered photons to be redshifted when viewed from the side. The bandpass filters described above are redshifted by 12% from the nominal harmonic wavelengths, to account for this effect. This mild redshift is convenient for discriminating against laser light and possible incidental (non redshifted) harmonics but not sufficiently strong to make scattered light viewed in the lab frame qualitatively different from that in the average electron rest frame.

Electron motion can become highly irregular as electrons are propelled radially from the tight laser focus by the ponderomotive force while oscillating during the pulse. This can grossly distort the emission patterns from individual electrons, depending on their initial positions in the focal volume and subsequent unique trajectory [16]. Nevertheless, when the emission is averaged from many electrons randomly distributed through the focus and over many laser shots, the emission converges to a pattern remarkably similar to those shown in Fig. 2. The theoretical curves in the next section are computed averages of photon emission from several thousand representative electron with initial positions distributed within the collection volume of our imaging system.

4. Measurements

Figure 4 shows measured Thomson scattering of the (redshifted) fundamental at various latitudes around the emission sphere. The scattered light is resolved into longitudinal and azimuthal polarization components. The angular emission pattern follows the expected dipole radiation distribution, which naturally exhibits both polarization components well away from the equatorial plane. This pattern is qualitatively similar to expected scattering angular profile for linear Thomson scattering observed at low intensity.

The measurements are compared with the simulated number of photons (from 600 laser shots) detected from the ensemble of electrons randomly distributed throughout the focal volume, summed incoherently. The simulations for Figs. 4–6 are performed as outlined in section 2, taking into account gas pressure, photon collection geometry, and detection efficiency as outlined in the preceding section. The simulation was conducted using representative values for the photon collection efficiency, but this collection efficiency varies due to alignment at each collection location. To account for these differences and to aid in comparing the measurements to theory the theoretical curves are scaled by a different factor at each location, reported as the "scaling" on each individual graph.

Figure 5 shows measured nonlinear Thomson scattering of the (red-shifted) second harmonic at various latitudes around the emission sphere. As before, the scattered light is resolved into longitudinal and azimuthal polarization components. As described in Ref. [33], the very different angular patterns for the two polarizations seen in Fig. 5 are associated with different dimensions of the figure-8 motion executed by the relativistic free electrons. In the equatorial plane ($\theta = 90°$), the $\hat{\boldsymbol{\theta}}$ component of the scattered light is exclusively associated with the $\hat{\mathbf{x}}$ component of electron motion, while the $\hat{\boldsymbol{\phi}}$ component is exclusively associated with the $\hat{\mathbf{z}}$ component of motion.

A dramatic difference can be seen in the emission patterns measured above and below the equatorial plane, which is the primary focus of this paper. For example, comparing second-harmonic emission at latitudes 45° and 135°, we see that the $\hat{\boldsymbol{\theta}}$ component of the scattered light is about five times stronger in the southern hemisphere than in the northern. We interpret this as being due to the asymmetry in the z-component of the velocity as electrons execute the figure-8 motion. The relative strengths of the two polarization components also vary between the two hemispheres. The good match between theory and experiment in both the pattern and the relative strength of the two polarizations at each θ gives evidence that the differences in signal strength are not due to misalignments of the detection system.

Optics EXPRESS

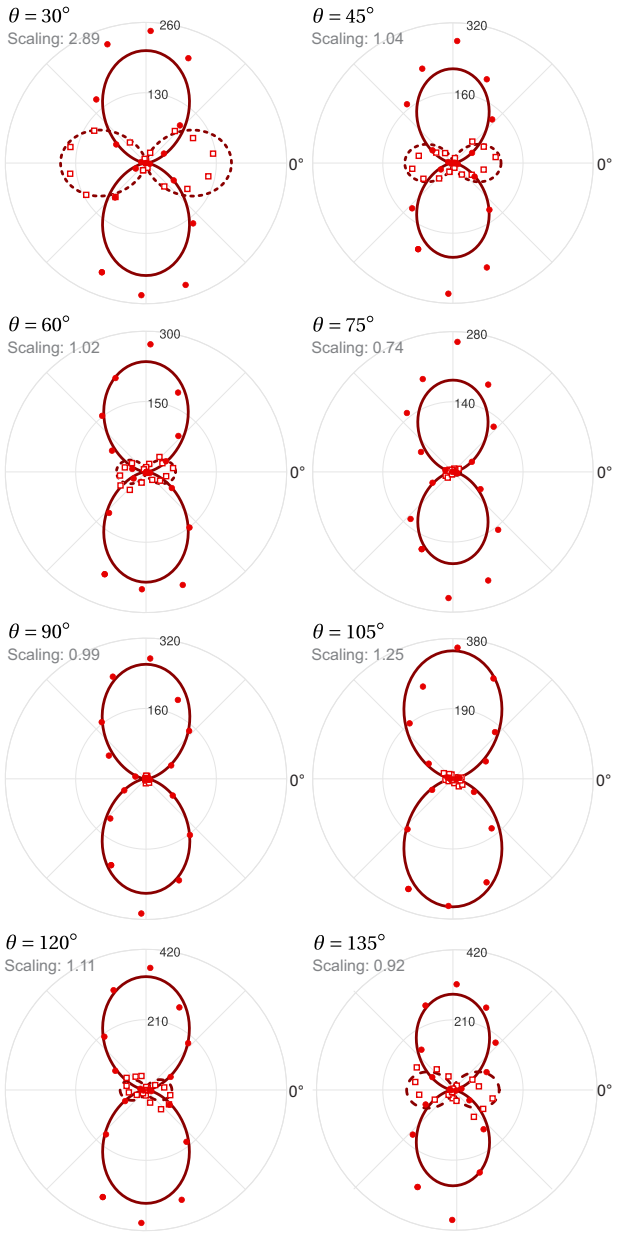

Fig. 4. Photon counts per 100 s for the fundamental (transmitted through a 900 nm filter) as a function of longitudinal angle. Open squares correspond to measured azimuthal polarization and filled circles to longitudinal polarization. Computationally modeled data are shown with dashed and solid curves, respectively. Scans are repeated at various latitudes referenced to the direction of laser propagation (at $\theta = 0°$). The computational model is first calculated using measured parameters (gas pressure, laser intensity, etc.) with no fitting parameters, and then multiplied by a scaling factor (reported in each frame) chosen to minimize the difference between measurement and computational model. The variation in scaling between frames likely results from variation in collection efficiency from our measured value due to the challenge of aligning the collection lenses at each angular position.

Optics EXPRESS

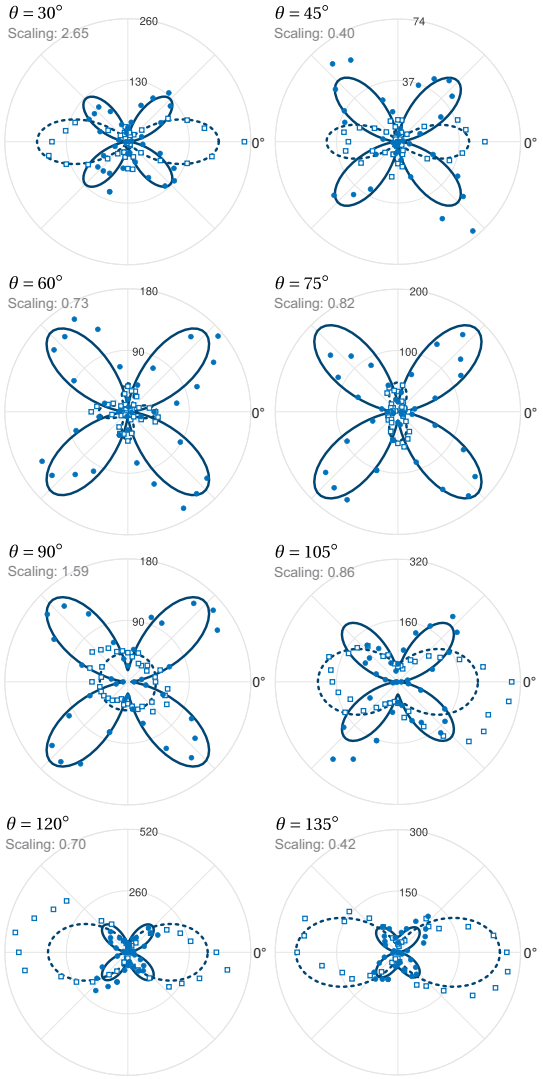

Fig. 5. Plots similar to those in Fig. 4 for second harmonic (transmitted through a 450 nm filter).

Figure 6 shows measured nonlinear Thomson scattering of the (redshifted) third harmonic at various latitudes around the emission sphere. Both polarization components of the scattered light are displayed as before. The asymmetry between the two hemispheres is also evident for this harmonic. For $\theta = 30^\circ$ and $\theta = 45^\circ$ we were unable to experimentally measure signal above the noise threshold. This measurement is in keeping with the calculated prediction of less than one photon in 600 shots as shown in theoretical curves for these angles.

Optics EXPRESS

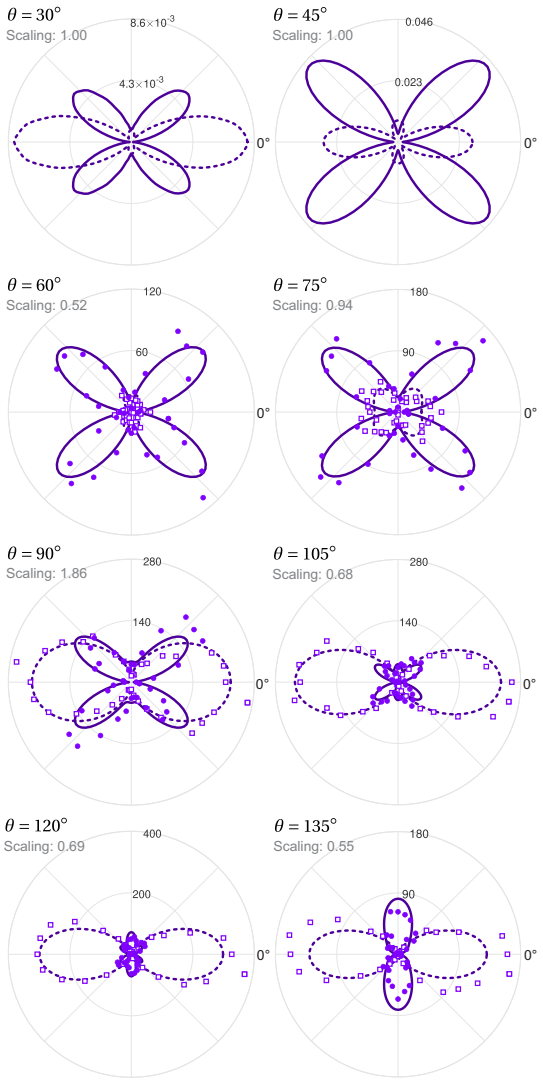

Fig. 6. Plots similar to those in Fig. 4 for third harmonic (transmitted through a 310 nm filter). No measured values were possible at $\theta = 30°$ or $\theta = 45°$ due to the very low signal level.

5. Conclusions

In a previous publication [33], we demonstrated the two-dimensional nature of the electron motion responsible for nonlinear Thomson scattering, consistent with the figure-8 trajectory in the case of linearly polarized laser field. In that work, we noted that mere one-dimensional motion (along the laser polarization) is sufficient to produce the $\hat{\boldsymbol{\phi}}$ polarization component of the scattered light (i.e. the clover or butterfly patterns in Figs. 5 and 6). To explain the emission with polarization along $\hat{\boldsymbol{\theta}}$ (i.e. the oblong patterns), the electron motion must also include a component along the direction of laser propagation.

In this work, we have demonstrated that the two-dimensional trajectory of the electron includes an asymmetry in the velocity component along the direction of laser propagation, giving rise to markedly different emission in the two hemispheres. The asymmetry is inherent to the figure-8

Optics EXPRESS

shape. As seen in Fig. 1, an electron travels opposite the direction of laser propagation on both ends of the figure-8, while it possesses a forward component of velocity for either path where they cross in the middle. The motion at the ends of the figure-8 involve greater acceleration, which is associated with brighter emission, whereas the acceleration in the middle is smaller and even momentarily zero. The velocity and acceleration are displayed in the animation of Fig. 1. The electron whips around both ends of the figure-8 while traveling opposite to the laser propagation.

If instead of following the crossing figure-8 trajectory, the electron followed, say, an oval path as depicted by a dashed line in Fig. 7(c), it would travel in opposite directions on the two ends of the trajectory. This hypothetical oval-shaped electron path is chosen to have similar velocity and acceleration to the actual figure-8 motion, but with the crossing in the middle removed. Figures 7(a) and (b) compare calculated emission between this hypothetical trajectory (dashed lines) and the actual trajectory (solid lines) for second harmonic emission in the 'northern' and 'southern' hemispheres at ±30° from the equator. The emission from the hypothetical oval is seen to be identical for both scattered polarizations. On the other hand, the figure-8 path shows the significant difference between the two hemispheres as shown in our measurements.

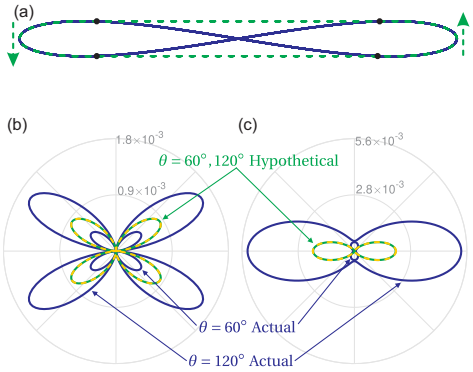

Fig. 7. (a) The actual figure-8 trajectory (solid) and a hypothetical electron trajectory (dashed) for which z-acceleration is artificially switched off between the upper and lower sets of indicated points, resulting in an oval-shape trajectory. Second harmonic emission calculated for the actual figure-8 motion at $\theta = 60°$ and $\theta = 120°$ is shown in (b) and (c) for azimuthal and longitudinal emission polarization, respectively (in units of eV per steradian).The emissions for the altered trajectory are also shown in (b) and (c), again for $\theta = 60°$ and $\theta = 120°$. Note that the altered trajectory does not exhibit asymmetry in emission between the northern and southern hemisphere of emission.

Finally, we can verify the directional sense that the electron travels around its figure-8 race track. The extra emission in the southern hemisphere indicates that the electron travels opposite to the laser propagation as it undergoes the acceleration on the ends of the figure-8. On the other hand, in the middle of the figure-8, the z component of electron motion moves with the laser propagation, as the electron oscillates primarily in the direction of laser polarization.

Funding. National Science Foundation (2207737).

Disclosures. The authors declare no conflicts of interest.

Data availability. Data underlying the results presented in this paper are not publicly available at this time but may be obtained from the authors upon reasonable request.

References

1. L. D. Landau and E. M. Lifshitz, *The Classical Theory of Fields*, (Addison-Wesley Press, Cambridge, 1951), 1st ed. pp. 120–121.
2. Vachaspati, "Harmonics in the Scattering of Light by Free Electrons," Phys. Rev. **128**, 664–666 (1962).

Optics EXPRESS

3. H. Eberly Joseph and Sleeper Arthur, "Trajectory and Mass Shift of a Classical Electron in a Radiation Pulse," Phys. Rev. **25**, 1570–1573 (1968).
4. E. S. Sarachik and G. T. Schappert, "Classical Theory of the Scattering of Intense Laser Radiation by Free Electrons," Phys. Rev. D **1**(10), 2738–2753 (1970).
5. A. K. Puntajer and C. Leubner, "Classical versus semiclassical predictions for harmonic generation in laser-free electron scattering under experimentally realizable conditions," J. Appl Phys. **67**, 1606–1609 (1990).
6. U. Mohideen, H. W. K. Tom, R. R. Freeman, *et al.*, "Interaction of free electrons with an intense focused laser pulse in Gaussian and conical axicon geometries," J. Opt. Soc. Am. B **9**(12), 2190 (1992).
7. E. Esarey, S. K. Ride, and P. Sprangle, "Nonlinear Thomson scattering of intense laser pulses from beams and plasmas," Phys. Rev. E **48**, 3003–3021 (1993).
8. C. I. Castillo-Herrera and T. W. Johnston, "Incoherent harmonic emission from strong electromagnetic waves in plasmas," IEEE Trans. on Plasma Sci. **21**(1), 125–135 (1993).
9. S. K. Ride, E. Esarey, and M. Baine, "Thomson scattering of intense lasers from electron beams at arbitrary interaction angles," Phys. Rev. E **52**(5), 5425–5442 (1995).
10. F. V. Harternann, S. N. Fochs, G. P. Le Sage, *et al.*, "Nonlinear ponderomotive scattering of relativistic electrons by an intense laser field at focus," Phys. Rev. E **51**, 4833–4843 (1995).
11. Y. I. Salamin and F. H. M. Faisal, "Harmonic generation by superintense light scattering from relativistic electrons," Phys. Rev. A **54**(5), 4383–4395 (1996).
12. Y. I. Salamin and F. H. M. Faisal, "Generation of Compton harmonics by scattering linearly polarized light of arbitrary intensity from free electrons of arbitrary initial velocity," J. Phys. A: Math. Gen. **31**(4), 1319–1327 (1998).
13. Y. Li and S. V. Milton, "Intensity and Pulse Shape Effect on the Spectra and the Angular Distribution of Nonlinear Thomson Scattering," *Conference on Lasers and Electro-Optics CLEO, OSA Technical Digest, CWA30* (2002).
14. Q-H. Park, R. W. Boyd, J. E. Sipe, *et al.*, "Theory of Relativistic Optical Harmonic Generation," IEEE J. of Selected Topics in Quantum Electronics **8**, 413–417 (2002).
15. F. He, Y. Y. Lau, D. P. Umstadter, *et al.*, "Backscattering of an Intense Laser Beam by an Electron," Phys. Rev. Lett. **90**(5), 055002 (2003).
16. J. Gao, "Thomson Scattering from Ultrashort and Ultraintense Laser Pulses," Phys. Rev. Lett. **93**(24), 243001 (2004).
17. G. A. Krafft, "Spectral Distributions of Thomson-Scattered Photons from High-Intensity Pulsed Lasers," Phys. Rev. Lett. **92**(20), 204802 (2004).
18. M. Boca and A. Oprea, "Thomson scattering in the high intensity regime," Phys. Scr. **83**(5), 055404 (2011).
19. S. G. Rykovanov, C. G. R. Geddes, C. B. Schroeder, *et al.*, "Controlling the spectral shape of nonlinear Thomson scattering with proper laser chirping," Phys. Rev. Accele. Beams **19**(3), 030701 (2016).
20. K. Ta Phuoc, A. Rousse, M. Pittman, *et al.*, "X-Ray Radiation from Nonlinear Thomson Scattering of an Intense Femtosecond Laser on Relativistic Electrons in a Helium Plasma," Phys. Rev. Lett. **91**(19), 195001 (2003).
21. K. Ta Phuoc, F. Burgy, J.-P. Rousseau, *et al.*, "Nonlinear Thomson scattering from relativistic laser plasma interaction," Eur. Phys. J. D **33**(2), 301–306 (2005).
22. M. Babzien, I. Ben-Zvi, K. Kusche, *et al.*, "Observation of the Second Harmonic in Thomson Scattering from Relativistic Electrons," Phys. Rev. Lett. **96**(5), 054802 (2006).
23. T. Kumita, Y. Kamiya, M. Babzien, *et al.*, "Observation of the Nonlinear Effect in Relativistic Thomson Scattering of Electron and Laser Beams," Laser Phys. **16**(2), 267–271 (2006).
24. G. Sarri, D. J. Corvan, W. Schumaker, *et al.*, "Ultrahigh Brilliance Multi-MeV γ-Ray Beams from Nonlinear Relativistic Thomson Scattering," Phys. Rev. Lett. **113**(22), 224801 (2014).
25. K. Khrennikov, J. Wenz, A. Buck, *et al.*, "Tunable All-Optical Quasimonochromatic Thomson X-Ray Source in the Nonlinear Regime," Phys. Rev. Lett. **114**(19), 195003 (2015).
26. Y. Sakai, I. Pogorelsky, O. Williams, *et al.*, "Observation of redshifting and harmonic radiation in inverse Compton scattering," Phys. Rev. ST Accel. Beams **18**(6), 060702 (2015).
27. W. Yan, C. Fruhling, G. Golovin, *et al.*, "High-order multiphoton Thomson scattering," Nat. Photonics **11**(8), 514–520 (2017).
28. T. J. Englert and E. A. Rinehart, "Second-harmonic photons from the interaction of free electrons with intense laser radiation," Phys. Rev. A **28**(3), 1539–1545 (1983).
29. S.-Y. Chen, A. Maksimchuk, and D. Umstadter, "Experimental observation of relativistic nonlinear Thomson Scattering," Nature **396**(6712), 653–655 (1998).
30. S.-Y. Chen, A. Maksimchuk, E. Esarey, *et al.*, "Observation of Phase-Matched Relativistic Harmonic Generation," Phys. Rev. Lett. **84**(24), 5528–5531 (2000).
31. M. Iinuma, K. Matsukado, I. Endo, *et al.*, "Observation of second harmonics in laser-electron scattering using low energy electron beam," Phys. Lett. A **346**(4), 255–260 (2005).
32. C. Z. He, A. Longman, J. A. Pérez-Hernandez, *et al.*, "Towards an in situ, full-power gauge of the focal-volume intensity of petawatt-class lasers," Opt. Express **27**(21), 30020 (2019).
33. B. Pratt, N. Atkinson, D. Hodge, *et al.*, "Experimental Confirmation of Electron Figure-8 Motion in a Strong Laser Field," Phys. Rev. A **103**(3), L031102 (2021).
34. C. Fruhling, J. Wang, D. Umstadter, *et al.*, "Experimental observation of polarization-resolved nonlinear Thomson scattering of elliptically polarized light," Phys. Rev. A **104**(5), 053519 (2021).

Optics EXPRESS

35. W. L. Erikson and S. Singh, "Polarization properties of Maxwell-Gaussian laser beams," Phys. Rev. E **49**(6), 5778–5786 (1994).
36. J. Peatross, M. Berrondo, D. Smith, *et al.*, "Vector fields in a tight laser focus: comparison of models," Opt. Express **25**(13), 13990 (2017).
37. J. D. Jackson, *Classical Electrodynamics*, 3rd ed. (Wiley, New York, 1998), Eqs. (11.124), (11.168), (14.14).